An experimental investigation of oil-water flow in a serpentine channel

Oguzhan Der, Volfango Bertola*

Laboratory of Technical Physics, School of Engineering, University of Liverpool, Brownlow Hill, Liverpool L69 3GH, United Kingdom

Abstract

The co-current oil-water flow in a horizontal serpentine channel is studied experimentally by high-speed imaging. Due to the channel geometry, the flow exhibits curved streamlines, which can induce secondary flows and alter the flow pattern transition boundaries in comparison with those observed in straight channels. This can have important applications in the development of microfluidic mixing devices. The serpentine channel was cut out in a black polypropylene sheet sandwiched between two transparent polypropylene sheets and bonded by selective laser welding. Different flow patterns were generated by changing independently the superficial velocities of the two fluids using a dual-drive syringe pump. Results enable the construction of a flow pattern map, which shows significant differences with the equivalent map obtained for straight microchannels.

Keywords: Liquid-liquid flow, Oil-water flow, Serpentine channel, Flow patterns
2010 MSC: 00-01, 99-00

1. Introduction

Co-current flows of two immiscible liquids are common in food, pharmaceutical, personal and health care products, as well as in many industrial formulations. In particular, oil-water two-phase flows in microfluidic devices have been successfully employed in creating emulsions commonly used in the chemical and textile industries, food, and many other domains. In these applications, controlling the size distribution and polydispersity of the dispersed phase can improve significantly the characteristics of the final product (Tan et al., 2008).

Early studies on liquid-liquid flows focused mainly on oil-water systems in straight pipes of circular cross section, with diameters ranging between 1 cm and 10 cm (Brauner, 2003). Later on, there was a growing interest in capillary tubes of millimetric diameter to investigate the flow behaviour in micro-gravity

*Corresponding author
Email address: Volfango.Bertola@liverpool.ac.uk (Oguzhan Der, Volfango Bertola)

conditions (Beretta et al., 1997). More recently, investigations of the hydrodynamics and mass transfer aspects of liquid-liquid two phase flow have been extended to micro-channels with diameters < 1 mm, for their relevance in bio- and micro-fluidic applications (Burns and Ramshaw, 2001; Kashid and Agar, 2007). Experimental parameters include the inlet geometry (e.g. T-type and Y-type), the micro-channel cross-sections (e.g. square, rectangular and circular), flow rates and the flow ratio, and the physical properties of the fluids. The majority of works was limited to low flow velocities where surface forces dominate, in which intermittent flow patterns are generally observed.

The first step in the study of a liquid-liquid flow system requires the identification of flow patterns, which can be classified into four basic morphologies: (i) stratified layers with either smooth or wavy interface; (ii) large slugs, elongated or spherical, of one liquid in the other; (iii) a dispersion of relatively fine drops of one liquid in the other; (iv) annular flow, where one of the liquids forms the core and the other liquid flows in the annulus. In many cases, however, the flow pattern consists of a combination of these basic morphologies (Dessimoz et al., 2007). The identification of the flow pattern is usually based on visual observations, photographic/imaging techniques, or on abrupt changes in the average system pressure drop, sometimes combined with conductivity measurements or high frequency impedance probes for local holdup sampling, or local pressure fluctuations and average holdup measurements (Bertola, 2003).

Oil-in-water flow patterns and slug hydrodynamics were experimentally studied in rectangular and square glass micro-channels of different hydraulic diameters ranging between 200 μm and 600 μm (Cao et al., 2018). The three main flow patterns observed were annular flow, slug flow and droplet flow, and general flow pattern transition criteria were proposed based on the Reynolds and the Weber numbers. In addition, a scaling law was proposed to predict the slug length, while the slug velocity was shown to be a linear function of the bulk velocity of the two phases. Flow pattern maps for the same systems were produced as a function of the flow rates ratio and the Capillary number of the dispersed phase (Wu et al., 2017). Alternatively, flow pattern maps can be reported as a function of the Reynolds and the Capillary numbers (Kashid and Kiwi-Minsker, 2011).

Experiments on liquid-liquid flow of different fluids in a square microchannel (200 μm hydraulic diameter) concluded that flow pattern maps based on Weber numbers cannot be generalised, and propose to introduce the product of the Weber and Ohnesorge numbers to as universal parameter to generalise flow maps (Yagodnitsyna et al., 2016).

Fluid mixing can be enhanced by fluid breakup in chaotic liquid-liquid flows (Muzzio et al., 1991). Chaotic fluid mixing can be obtained, for example, by means of secondary flow induced by curved streamlines (Castelain et al., 2001). Thus, one can build a simple, continuous flow chaotic mixer using a long serpentine channel. Adding complexity to the flow field has potential to increase the amount of mixing also in microchannels with zigzag geometry (Branebjerg et al., 1995) and three-dimensional serpentine channels designed to introduce chaotic advection into the system and further enhance mixing over a 2-D ser-

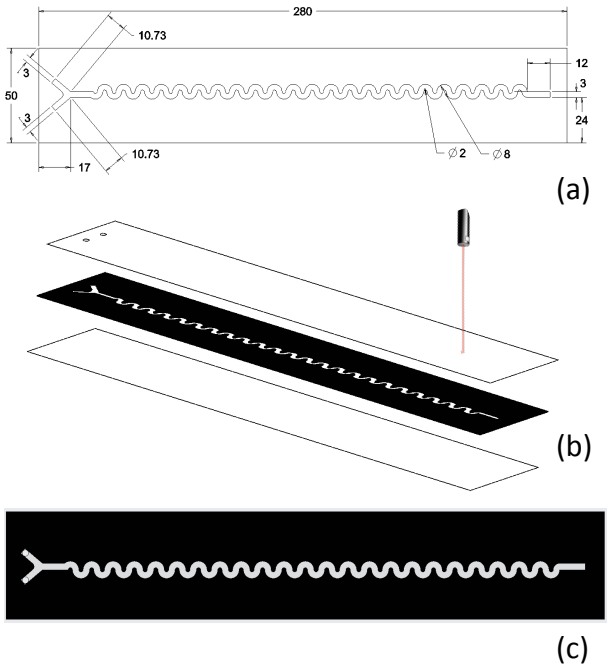

Figure 1: Schematic of the test section: (a) dimensions of the serpentine channel (in mm); (b) schematic of the laser welding process; (c) assembled test section

pentine channel (Liu et al., 2000). Whilst these studies concern single-phase flows, the literature about liquid-liquid flows in serpentine or coiled channels is very limited (Sarkar et al., 2012; Wu and Sundén, 2018).

The present work investigates experimentally the co-current oil-water flow in a polypropylene serpentine mini-channel of millimetric size with a square cross-section. Fluidic devices built with polymer materials have an important role in emerging and perspective applications such as portable electronics, chemical reactors, soft robotics and deployable systems, where the use of metallic channels is limited due to cost, weight and mechanical flexibility constraints (Der et al., 2019a,b; Maleki and Bertola, 2019). Flow patterns were identified by high-speed imaging, and flow pattern maps were constructed with respect to different flow parameters and compared with those reported in the literature for straight channels.

2. Experimental setup and procedure

2.1. Test section design and fabrication

The test section consisted of a polypropylene serpentine channel having a square cross section with a width $L = 3$ mm, consisting of a sequence of 46

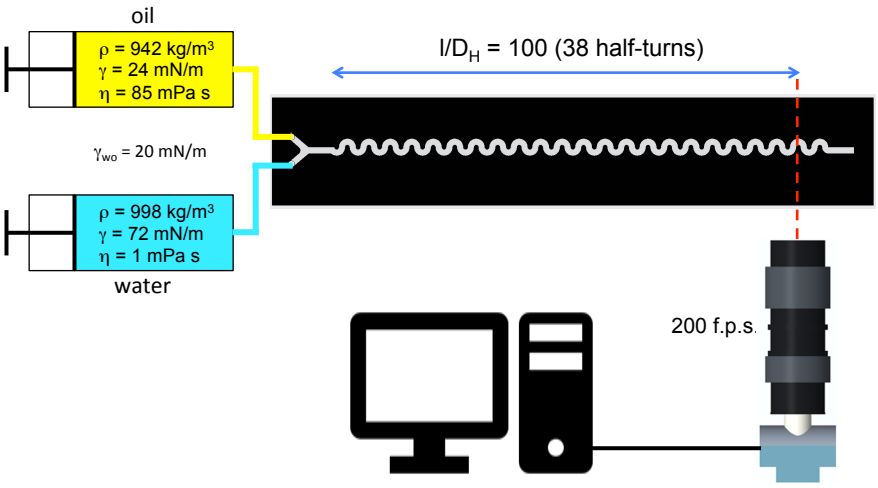

Figure 2: Schematic of the experimental setup displaying the two-channel syringe pump (SP), the test section with a water inlet (WI), an oil inlet (OI), and an oil-water outlet (OWO), the LED illumination sys- tem (LED), and the high-speed camera (HSC) con- nected to a computer equipped with frame grabber (PC).

circular half turns, with inner and outer radii of 1 mm and 4 mm, respectively, as shown in Figure 1a.

The channel had two inlets, respectively for oil and water, merging together through a Y-junction, and one outlet. The channel shape was cut out into the black polypropylene sheet (3 mm thickness) using a LS1290 PRO Laser Cutter (maximum power: 80 W; cutting area: 1200 mm x 900 mm). The quality of the cut was determined mainly by the kerf width, which was kept as small as possible, and the roughness of the cut edge (Choudhury and Shirley, 2010). To improve the cut edge finish, cutting was carried out repeating several engraving passes, removing approximately 0.1 mm of material at each pass. The surface of the cut polypropylene sheet was washed with an ethanol and distilled water to remove dust and impurities.

The channel was then sealed between two sheets of clear polypropylene (0.4 mm thickness each) by laser transmission welding (Amanat et al., 2010), using a nanosecond pulsed fibre laser (SPI G4 HS-L 20W) with a wavelength of 1064 nm and pulse repetition rate of 500 kHz. In this process, the laser beam goes through the clear transmissive layer and is absorbed by the adjacent black layer, melting the two sheets exactly at the interface (Humbe et al., 2014) as shown schematically in figure 1b.

2.2. Experimental setup

A schematic of the experimental layout is displayed in Figure 2. The two fluids (water and a commercial vegetable oil) were dispensed independently at

controlled rate using a programmable syringe pump with dual drive system (Chemyx Fusion 4000). To minimise the transient inertial effects, the syringes were connected to the test section inlets by rigid nylon tubes.

Flow patterns were observed through the transparent walls of the channel using a colour high-speed CMOS camera (Mikrotron MC1310) placed above the channel, and equipped with a 18-108/2.5 zoom lens (Navitar Zoom 7000), with a resolution of 1280 x 440 pixels, at the rate of 200 frames per second. A single 3 W LED backlight equipped with diffuser was used to ensure uniform illumination and enhance the fluid interface contrast. The camera was placed at a distance from the inlet corresponding to 38 half-turns, i.e., 100 hydraulic diameters, to ensure the flow was fully developed.

For each fluid the flow rates, respectively $\dot{V}_o$ for oil and $\dot{V}_w$ for water, were varied between 0.5 mL/min and 5 mL/min, with increments of 0.5 mL/min; correspondingly, the superficial velocities, defined as $J_w = \dot{V}_w/L^2$ and $J_o = \dot{V}_o/L^2$ ranged between 0.926 mm/s and 9.26 mm/s.

2.3. Fluid properties and flow parameters

The fluid densities, measured by weighing a fixed volume of fluid with a precision analytical balance (Mettler Toledo), were $\rho_w = 998$ kg/m^3 and $\rho_o = 942$ kg/m^3 for water and oil, respectively. The fluid viscosities, measured with capillary viscometer (Schott Gerate) were $\eta_w = 1$ mPa·s and $\eta_o = 85$ mPa·s for water and oil, respectively. A Krüss EasyDyne tensiometer equipped with a Wilhelmy plate probe was used to measure the surface tensions of the two fluids, as well as their interfacial tension at the ambient temperature of 20°C. The fluid surface tensions were $\gamma_w = 72.8$ mN/m and $\gamma_o = 24.4$ mN/m for water and oil, respectively, while the interfacial tension was $\gamma_{wo} = 20.1$ mN/m. Correspondingly the capillary length, defined as:

$$a = \sqrt{\frac{\gamma_{wo}}{(\rho_w - \rho_o)\, g}} \tag{1}$$

was $a = 6.05$ mm, while the Eötvös number, defined as:

$$Eo = \frac{(\rho_w - \rho_o)\, g L^2}{\gamma_{wo}} \tag{2}$$

where $L = 3$ mm is the size of the channel cross section, was $Eo = 0.246$, which indicates that the interfacial tension dominates the flow.

The other relevant dimensionless parameters, i.e. the Capillary number, the Reynolds number, the Weber number, and the Ohnesorge number, were calculated respectively as:

$$Ca_{w,o} = \frac{\eta_{w,o} J_{w,o}}{\gamma_{wo}} \tag{3}$$

$$Re_{w,o} = \frac{\rho_{w,o} J_{w,o} L}{\eta_{w,o}} \tag{4}$$

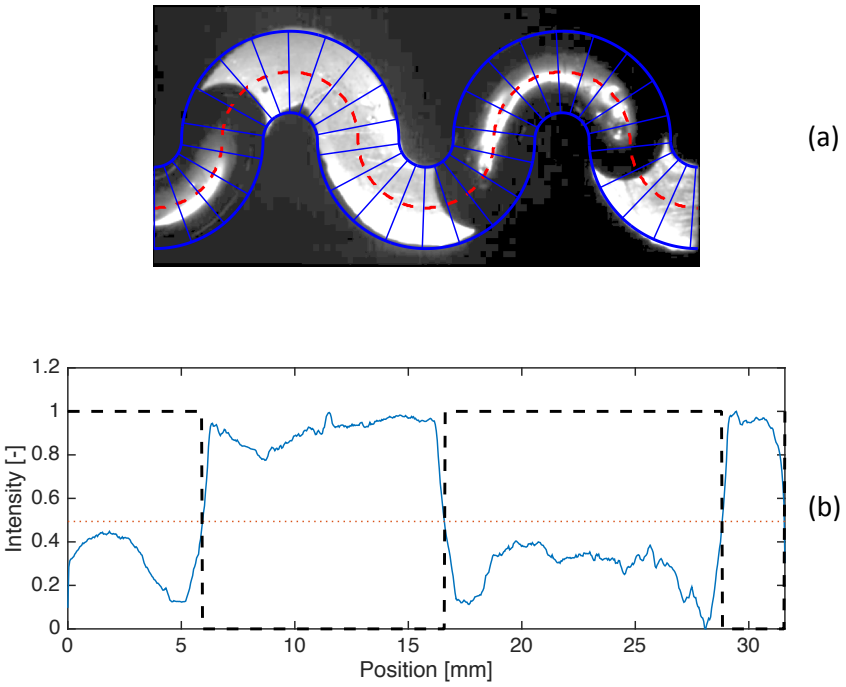

Figure 3: Image processing procedure: (a) contrast enhanced image with reference grid (only 1/20th of the radial lines are displayed for clarity); (b) normalized intensity profile (solid line), average intensity (dotted line), and binary square wave (dashed line).

$$We_{w,o} = \frac{\rho_{w,o} J_{w,o}^2 L}{\gamma_{wo}} \tag{5}$$

$$Oh_{w,o} = \frac{\sqrt{We_{w,o}}}{Re_{w,o}} \tag{6}$$

Finally, the equilibrium contact angles (de Gennes, 1985) of the two fluids on a polypropylene surface, measured from side views of sessile drops using a standard optical goniometer with digital image processing software (Biolè and Bertola, 2015; Biolè et al., 2016), were $\theta_w = 50.1° \pm 1°$ and $\theta_o = 21.9° \pm 1°$ for water and oil, respectively.

2.4. Image processing

Measurements of the slug length and velocity were obtained by digital image processing. First, each image was converted to grayscale and filtered with a 2D Gaussian smoothing kernel with standard deviation of 0.8. The image contrast was enhanced by mapping intensity values within the range between 0 and 0.4 into the full intensity scale (i.e., between 0 and 1) according to a power-law

relationship with exponent equal to 0.4. Then, a mask displaying the channel walls and a grid formed by the centerline with the half-turn radii was applied to the image, as shown in Figure 3a. The image intensity was averaged along the half-turn radii and plotted as a function of the curvilinear abscissa measured along the centerline, s, as shown in Figure 3b. The averaged image intensity, $I_{av}(s)$, was then converted to a binary square wave as:

$$B(s) = \left[\frac{I_{av}(s) - \langle I_{av}(s) \rangle + |I_{av}(s) - \langle I_{av}(s) \rangle|}{2} \right] \tag{7}$$

Equation (7) represents the dispersed phase density function ($B(s) = 1$ if the cross-section at the curvilinear coordinate s is mainly occupied by water, and $B(s) = 0$ if it is mainly occupied by oil).

The slug length was obtained from the binary function $B(s)$, after removing the partial slugs which may be present at the beginnin and/or at the end of any frame. The cross-correlation of the function $I_{av}(s)$ at different times was used to calculate the slug velocity (Bertola, 2002). In particular, for each time series of images, the cross-correlation was carried out on all pairs of images with a lag of 50 frames (corresponding to 250 ms), which returned the most likely slug displacement occurring in this time lag; the ratio between the slug displacement and the time lag returns the most likely slug velocity.

3. Results

3.1. Flow patterns

The typical flow patterns observed during the oil/water flow are displayed in Figure 4. Since the polypropylene channel walls are moderately hydrophobic ($\theta_W = 50°$), oil was the continuous phase in all the flow conditions considered (water-in-oil dispersion). In contrast, most of the works reported in the existing literature use channels built with highly wettable materials, such as glass or metals (Garstecki et al., 2006; Wu et al., 2017; Cao et al., 2018), therefore a highly polar liquid such as water is observed to be the continuous phase. In particular, four different flow patterns were identified:

- *Droplet flow* when the drops of the dispersed phase (water) have a size, measured along the curvilinear direction of the flow, $D_l \leq a$ (Figure 4a).
- *Slug flow* when the dispersed phase takes the form of elongated slugs, having a length measured along the curvilinear direction of the flow $D_l > a$ (Figure 4b).
- *Slug/dispersed flow* when the gap between consecutive slugs is a homogeneous dispersion of water droplets with a diameter $D \ll a$ (Figure 4c).
- *Slug/annular flow* when water flows in chains of very long slugs extending over several turns of the serpentine channel, separated from the channel walls by a thin oil film; the oil phase also fills the gap between the rounded tail and head of two consecutive slugs (Figure 4d).

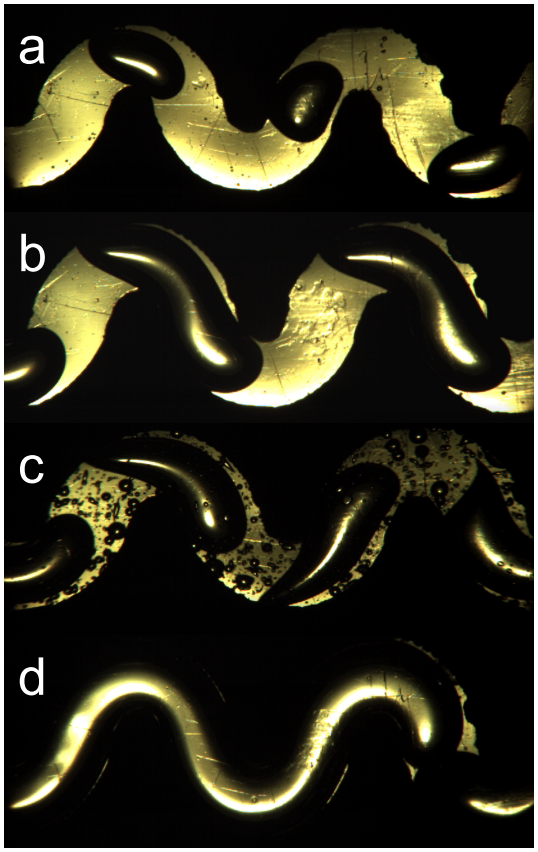

Figure 4: Flow patterns observed in the water-in-oil flow inside a serpentine channel with square cross-section (3 mm × 3 mm): (a) drop regime($\dot{V}_W$ = 1 ml/min, $\dot{V}_O$ = 3.5 ml/min); (b) slug flow ($\dot{V}_W$ = 2 ml/min, $\dot{V}_O$ = 2 ml/min); (c) slug/dispersed flow ($\dot{V}_W$ = 3.5 ml/min, $\dot{V}_O$ = 4 ml/min); (d) slug/annular flow ($\dot{V}_W$ = 5 ml/min, $\dot{V}_O$ = 2 ml/min).

The corresponding flow pattern maps are displayed in Figure 5; in particular, Figure 5a displays the map obtained using the superficial velocities of the two fluids as coordinates, while Figure 5b displays the same map using the dimensionless parameter $We{\cdot}Oh$ for the two phases as coordinates. This parameter arises from dimensional analysis arguments developed for the liquid-liquid flow in straight microchannels (Zhao et al., 2006; Yagodnitsyna et al., 2016). The solid lines in Figure 5b indicate the transition boundaries between the drop regime and the slug regime, and between the slug regime and the slug/dispersed regime, respectively. The transition boundary between the drop regime and the slug regime is well described by the following correlation:

$$(We \cdot Oh)_o = 500\,(We \cdot Oh)_w \tag{8}$$

while the transition boundary between the slug regime and the slug/dispersed

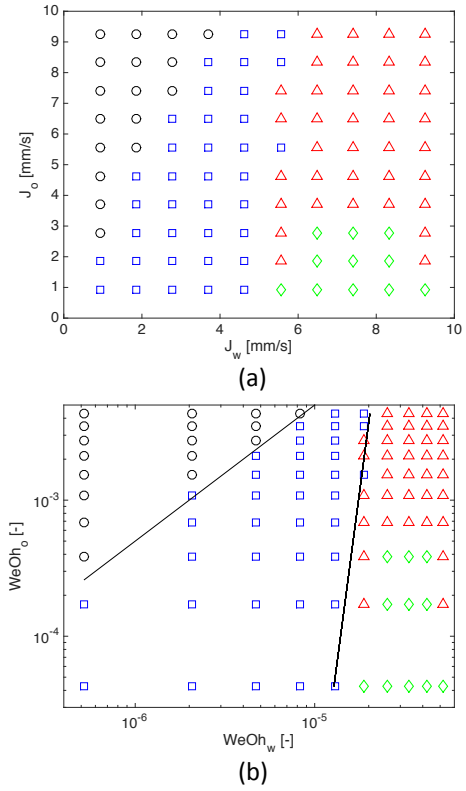

Figure 5: Flow pattern map for water-in-oil flow inside a serpentine channel with square cross-section (3 mm × 3 mm) plotted with respect to the superficial velocities of the fluids (a) and to the dimensionless variable WeOh (b); drop regime (○); slug flow (□); slug/dispersed flow (△); slug/annular (◇).

regime is given by:

$$(We \cdot Oh)_w = 3.5 \cdot 10^{-5} \, (We \cdot Oh)_o^{0.1} \tag{9}$$

These results confirm the dimensional analysis arguments used to analyse flow pattern transition in straight channels are applicable to the serpentine geometry. However, the comparison with the universal flow pattern map for straight microchannels (Yagodnitsyna et al., 2016), displayed in Figure 6, reveals a significant difference. In particular, the transition between parallel flow and droplet flow in the universal flow pattern map corresponds to the transition between droplet flow and slug flow observed in the serpentine channel, and is shifted towards lower value of the parameter $We \cdot Oh$ of the continuous phase (oil in the present work).

A second difference is the absence of parallel flow in the serpentine channel, where it is replaced by three flow patterns: slug flow, slug/dispersed flow, and slug/annular flow, with the points corresponding to slug/annular flow located

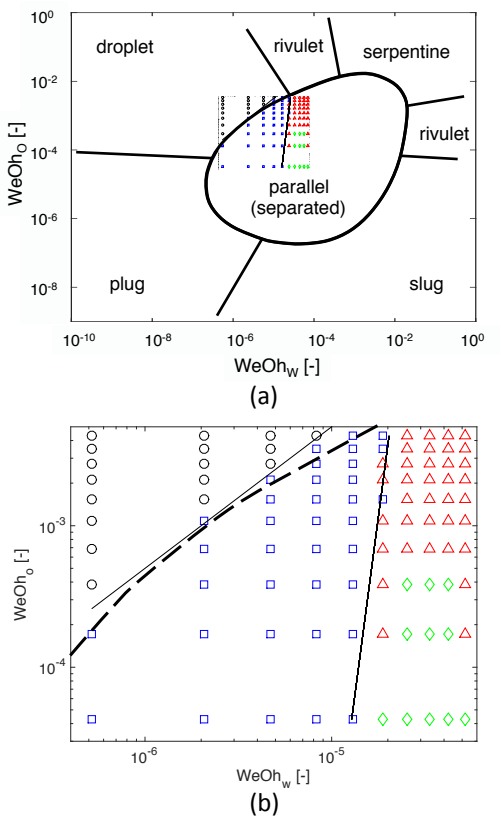

Figure 6: Comparison between the experimental flow pattern map for water-in-oil flow inside a serpentine channel with square cross-section (Figure 5) with the general flow pattern map plotted with respect to the dimensionless variables $(We \cdot Oh)_{oil}$ and $We \cdot Oh_{water}$ (Yagodnitsyna et al., 2016), displaying: drop regime (○); slug flow (□); slug/dispersed flow (△); slug/annular (◇). (a) full map; (b) detail of the droplet flow/parallel flow transition boundary.

approximately in the centre of parallel flow region of the universal map. This suggests the secondary flow induced by curved streamlines enhances mixing of the two phases, by disrupting the stability of parallel flow and replacing it with intermittent flow patterns.

The slug/annular flow, displayed in Figure 4d, is characterised by very long liquid slugs with only small amounts of oil between two consecutive slugs, therefore it could be regarded to as a pseudo-parallel flow regime. In this perspective, one can conclude the effect of the serpentine geometry is to shrink the region of parallel (i.e., separated) flow on the universal flow pattern map obtained for straight microchannels, expanding at the same time the region of intermittent and dispersed flows. This results into a moderate improvement in mixing the two phases in comparison with the flow in straight channels.

3.2. Intermittent regimes characterization

The main features of intermittent flow patterns (droplet flow, slug flow, and slug/dispersed flow) were analyzed based on the dispersed phase density function defined by Eq. (7). Figure 7 displays typical space-time diagrams for the three flow patterns, where bright and dark stripes correspond, respectively, to the water phase and the oil phase. The width of bright stripes, measured along the spatial axis, corresponds to the water drops (Figure 7a) or slugs (Figure 7b and 7c) size, while their slope represents the slug velocity. The diagram relative to the slug/dispersed regime (Figure 7c) features irregular edges and spots, which are the signature of the smaller water bubbles dispersed in the oil phase between two consecutive slugs (see Figure 4c).

The dimensionless drop and slug lengths, D_l/a, are plotted as a function of the ratio between the dispersed phase superficial velocity, J_w, and the total superficial velocity, $J_o + J_w$, in Figure 8a. In the droplet regime, the drop size is slightly smaller than the capillary length (Eq. 1), with the exception of the values obtained for the lowest water/oil ratios, where the number of water drops observed, however, is too small to be statistically significant. The ensemble of measured slug lengths is well described by the following correlation:

$$\frac{D_l}{a} = A + B\left(\frac{J_w}{J_o + J_w}\right)^n \tag{10}$$

where the coefficients A and B and the power-law index n can be determined by least-squares best fit.

An alternative scaling law, specifically developed to predict the size of droplets and bubbles produced in T-junction microchannels with $Ca \ll 1$, i.e., when the shear stress force is negligible and the slug length is defined only by the pressure distribution (Garstecki et al., 2006), expresses the dimensionless drop and slug length as a function of the superficial velocity ratio:

$$\frac{D_l}{L} = 1 + C\left(\frac{J_w}{J_o}\right) \tag{11}$$

where C is a fitting parameter of order one which depends on the inlet geometry. Figure 8b shows Eq. (11) can predict the drop and slug lengths in a serpentine channel with Y-junction inlet geometry provided the fitting parameter C is adjusted between 1.5 and 3.5. The partial mismatch is likely due to the influence of shear forces on the drop and slug pinch-off mechanism at the channel inlet, which becomes relevant at capillary numbers of the order of 10^{-2} (Garstecki et al., 2006; Yagodnitsyna et al., 2016).

Figure 9 shows the velocity of water drops and slugs plotted as a function of the total superficial velocity (i.e., the mean velocity of the two-phase mixture). For all of the three flow patterns considered, the drop and slug velocity (both in the slug and in the slug/dispersed flow regimes) is a linear function of the total superficial velocity, and its magnitude is slightly less than the maximum velocity of a single-phase flow in a square channel with mean velocity equal to the total superficial velocity of the two-phase mixture (Spiga and Morini, 1994).

This can be attributed to a better momentum transport in the channel cross-section, which confirms the moderate increase of mixing already observed from the analysis of flow pattern maps.

4. Conclusions

The two-phase flow of oil and water flow in a horizontal serpentine channel was investigated experimentally by high-speed imaging. Different flow regimes were identified depending on the superficial velocities of the two fluids, and sorted into an empirical flow pattern map. Flow pattern transitions were found to be a function of the product of the Weber and Ohnesorge numbers, in agreement with dimensional analysis arguments for straight channels.

The serpentine geometry enhances the fluids mixing with respect to straight channels, by reducing significantly the area of the separated flow region.

Finally, the slug length and velocity correlate, respectively, with the volumetric flow fraction of the dispersed phase and with the total superficial velocity of the mixture, irrespective of the flow pattern, and in agreement with the literature.

References

Amanat, N., James, N., McKenzie, D., 2010. Welding methods for joining thermoplastic polymers for the hermetic enclosure of medical devices. Med. Eng. Phys. 32, 690–699.

Beretta, A., Ferrari, P., Galbiati, L., Andreini, P., 1997. Oil-water flow in small diameter tubes. flow patterns. International Comm. Heat Mass Transfer 24, 223–229.

Bertola, V., 2002. Slug velocity profiles in horizontal gas-liquid flow. Experiments in Fluids 32, 722–727.

Bertola, V., 2003. Experimental characterization of gas-liquid intermittent subregimes by phase density function measurements. Experiments in Fluids 34, 122–129.

Biolè, D., Bertola, V., 2015. A goniometric mask to measure contact angles from digital images of liquid drops. Colloids and Surfaces A: Physicochemical and Engineering Aspects 467, 149–156.

Biolè, D., Wang, M., Bertola, V., 2016. Assessment of direct image processing methods to measure the apparent contact angle of liquid drops. Experimental Thermal and Fluid Science 76, 296–305.

Branebjerg, J., Fabius, B., Gravesen, P., 1995. Application of miniature analyzers: From microfluidic components to tas, in: van den Berg, A., Bergveld, P. (Eds.), Micro Total Analysis Systems. Kluwer Academic Publishers, Dordrecht, pp. 141–151.

Brauner, N., 2003. Liquid-liquid two-phase flow systems, in: Bertola, V. (Ed.), Modelling and Experimentation in Two-Phase Flow. Springer-Verlag, Wien. volume 450 of *CISM International Centre for Mechanical Sciences*. Chap. 5, pp. 221–279.

Burns, J., Ramshaw, C., 2001. The intensification of rapid reactions in multiphase systems using slug flow in capillaries. Lab on a Chip 1, 10–15.

Cao, Z., Wu, Z., Sundén, B., 2018. Dimensionless analysis on liquid-liquid flow patterns and scaling law on slug hydrodynamics in cross-junction microchannels. Chemical Engineering Journal 344, 604–615.

Castelain, C., Mokrani, A., Le Guer, Y., Peerhossaini, H., 2001. Experimental study of chaotic advection regime in a twisted duct flow. Eur. J. Mech. B - Fluids 20, 205–232.

Choudhury, I., Shirley, S., 2010. Laser cutting of polymeric materials: An experimental investigation. Optics-Laser Technology 42, 503–508.

Der, O., Edwardson, S., Marengo, M., Bertola, V., 2019a. Engineered composite polymer sheets with enhanced thermal conductivity. IOP Conference Series: Materials Science and Engineering 613, 012008.

Der, O., Marengo, M., Bertola, V., 2019b. Thermal Performance of Pulsating Heat Stripes Built With Plastic Materials. Journal of Heat Transfer 141.

Dessimoz, A., Raspail, P., Berguerand, C., Kiwi-Minsker, L., 2007. Quantitative criteria to define flow patterns in micro-capillaries. Chemical Engineering Journal 160, 882–890.

Garstecki, P., Fuerstman, M.J., Stone, H.A., Whitesides, G.M., 2006. Formation of droplets and bubbles in a microfluidic t-junction—scaling and mechanism of break-up. Lab Chip 6, 437–446.

de Gennes, P.G., 1985. Wetting: statics and dynamics. Reviews of Modern Physics 57, 827–863. URL: `http://link.aps.org/doi/10.1103/RevModPhys.57.827`.

Humbe, A., Deshmukh, P., Jadhav, C., Wadgane, S., 2014. Review of laser plastic welding process. International Journal of Research in Engineering - Technolog 2, 191–206.

Kashid, M., Agar, D., 2007. Hydrodynamics of liquid-liquid slug flow capillary microreactor: flow regimes, slug size and pressure drop. Chemical Engineering Journal 131, 1–13.

Kashid, M., Kiwi-Minsker, L., 2011. Quantitative prediction of flow patterns in liquid-liquid flow in micro-capillaries. Chemical Engineering and Processing 50, 972–978.

Liu, R., Stremler, M., Sharp, K., Olsen, M., Santiago, J., Adrian, R., Aref, H., Beebe, D., 2000. Passive mixing in a three-dimensional serpentine microchannel. J. MEMS 9, 190–197.

Maleki, H., Bertola, V., 2019. TiO2 nanofilms on polymeric substrates for the photocatalytic degradation of methylene blue. ACS Applied Nano Materials 2, 7237–7244.

Muzzio, F., Tjahjadi, M., Ottino, J., 1991. Self-similar drop-size distributions produced by breakup in chaotic flows. Physical Review Letters 67, 54–57.

Sarkar, P., Singh, K., Shenoy, K., Sinha, A., Rao, H., Ghosh, S., 2012. Liquid-liquid two-phase flow patterns in a serpentine microchannel. Ind. Eng. Chem. Res. 51, 5056–5066.

Spiga, M., Morini, G., 1994. A symmetric solution for velocity profile in laminar flow through rectangular ducts. International Communications in Heat and Mass Transfer 21, 469–475.

Tan, J., Xu, J., Li, S., Luo, G., 2008. Drop dispenser in a cross-junction microfluidic device: Scaling and mechanism of break-up. Chemical Engineering Journal 136, 306–311.

Wu, Z., Cao, Z., Sundén, B., 2017. Liquid-liquid flow patterns and slug hydrodynamics in square microchannels of cross-shaped junctions. Chemical Engineering Science 164, 56–66.

Wu, Z., Sundén, B., 2018. Liquid-liquid two-phase flow patterns in ultra-shallow straight and serpentine microchannels. Heat Mass Transfer , 1–14.

Yagodnitsyna, A., Kovalev, A., Bilsky, A., 2016. Flow patterns of immiscible liquid-liquid flow in a rectangular microchannel with t-junction. Chemical Engineering Journal 303, 547–554.

Zhao, Y., Chen, G., Yuan, 2006. Liquid-liquid two-phase flow patterns in a rectangular microchannel. AIChE Journal 52, 4052–4060.

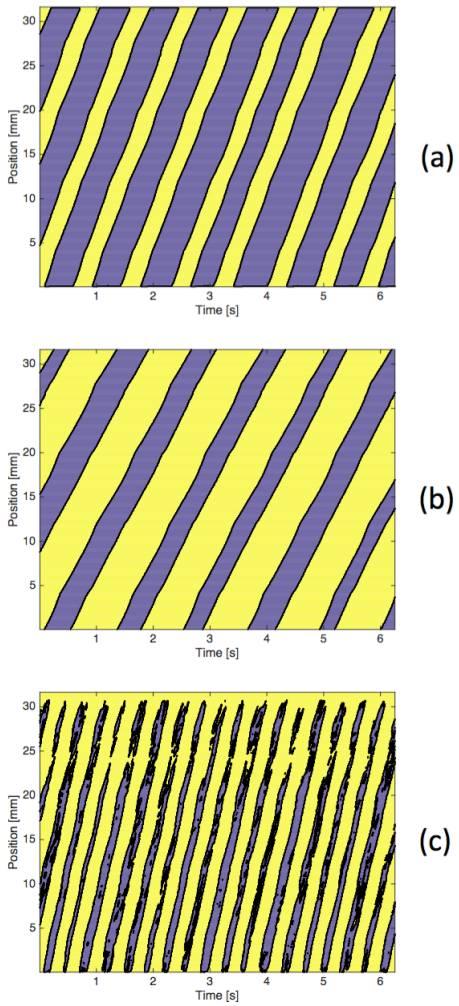

Figure 7: Examples of space-time diagrams obtained from the binary phase function (Eq. 7) measured on the centerline of the serpentine channel for droplet flow (a), slug flow (b) and slug/dispersed flow (c). Bright and dark stripes correspond, respectively, to the water phase and the oil phase. The slope of stripes represents the drop or slug velocity.

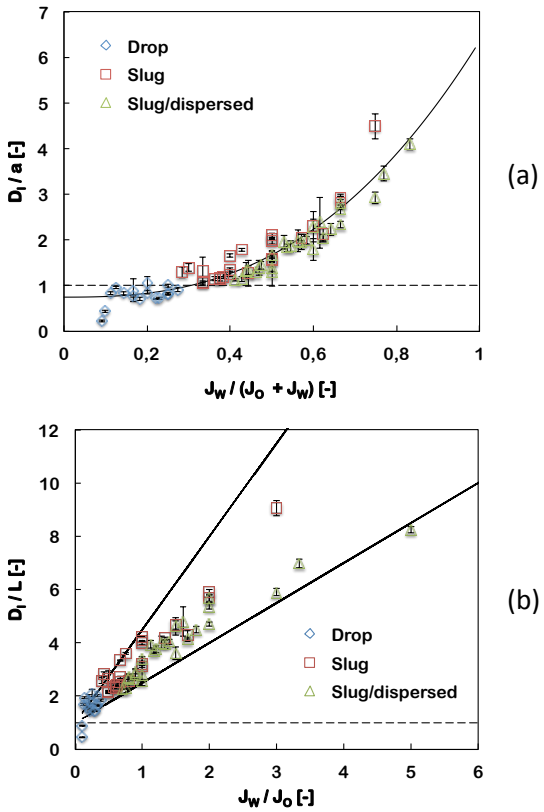

Figure 8: (a) Dimensionless drop and slug length plotted as a function of the ratio of the dispersed phase superficial velocity, J_w and the total superficial velocity, $J_o + J_w$; The solid line represents the least-squares best fit of Eq. (10), where $A = 0.75$, $B = 5.6$ and $n = 2.6$. (b) Dimensionless drop and slug length plotted as a function of the superficial velocity ratio, J_w/J_o; the solid lines represent Eq. (11) with $C = 1.5$ and $C = 3.5$, respectively, while the discontinuous line indicates the capillary length.

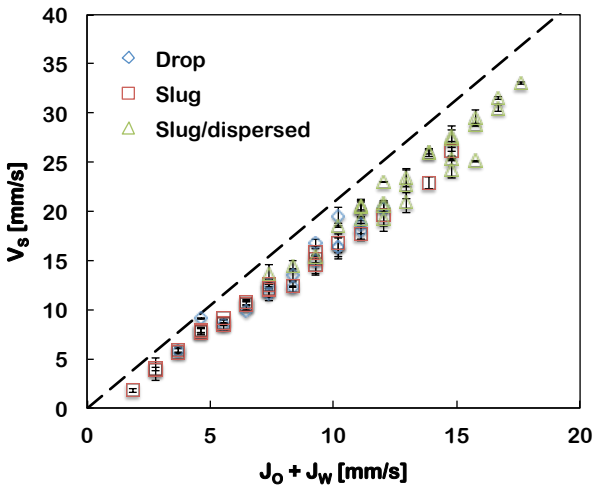

Figure 9: Drop and slug velocity plotted as a function of the total superficial velocity, $J_o + J_w$. The dashed line represents the maximum velocity of a single-phase flow in a square channel with a mean velocity equal to the total superficial velocity of the oil-water mixture (Spiga and Morini, 1994).